Comparison of Narrow Bipolar Events with Ordinary Lightning as Proxies for Severe Convection

ABRAM R. JACOBSON

Los Alamos National Laboratory, Los Alamos, New Mexico

MATHEW J. HEAVNER

Department of Physics, University of Alaska Southeast, Juneau, Alaska

(Manuscript received 10 March 2004, in final form 8 October 2004)

ABSTRACT

Narrow bipolar events (NBEs) are a recently studied intracloud electrical-discharge process. It is speculated that an NBE is instigated by the extensive atmospheric shower of an energetic cosmic ray. NBEs cause significant relaxation of the charge separation within the electrified cloud in a short time, on the order of 10 μs. The current flow causes radiation of a distinctive "bipolar" low-frequency/very low frequency signal that can be recorded at locations on earth up to thousands of kilometers from the source. NBEs are preceded/accompanied by the most powerful very high frequency radio emissions seen in any kind of lightning. These intense pulsed radio emissions have been routinely detected with satellite-borne radio receivers in space. Owing to their easy detection and recognition, NBEs might be a useful remote sensing proxy for space-based global, near–real time remote sensing. However, in order for that potential to be realized, NBEs must be shown to be associated, as is ordinary lightning, with severe tropospheric convection, rather than to be just a curiosity of cosmic-ray–atmosphere interactions. This question is addressed with a detailed comparison of NBEs and ordinary lightning using a ground-based lightning-transient research facility that records signals from both ordinary lightning and NBEs, the Los Alamos Sferic-waveform Array (LASA), based in Florida. First, the data from LASA are internally compared to examine the relationship of NBEs and ordinary lightning in both position and time. Second, the relationship of both NBEs and ordinary lightning to simultaneous infrared cloud imagery is examined [from the Geostationary Operational Environmental Satellite-East (GOES-East)] in order to infer the relative affinities of NBEs and ordinary lightning for cloud signatures that are consistent with severe convection.

1. Introduction and background

Space-based detection and location of lightning offers the potential for global, near–real time monitoring and tracking of severe deep convection. Space-based remote sensing offers, in principle, unhindered access to the entire planet. Lightning can be monitored from space by satellite-based detection of both optical (Boccippio et al. 2000; Christian et al. 1999a,b; Kirkland et al. 2001; Suszcynsky et al. 2000b, 2001) and radio-frequency (RF) emissions (Jacobson et al. 1999, 2000; Light and Jacobson 2002; Shao and Jacobson 2001, 2002).

Space-based RF monitoring of lightning can be done only at frequencies sufficiently high not to be blocked or overly dispersed by the ionosphere (Jacobson et al. 1999; Massey et al. 1998b; Roussel-Dupré et al. 2001). On the other hand, most lightning radio emissions have power spectra that roll off steeply versus frequency. In practice this means that the frequencies of observation must be in the very high frequency band (VHF; 30–300 MHz). The background of anthropogenic noise in the VHF forces lightning detection in space to exploit the most intense RF emissions, as only these can be triggered-upon while at the same time rejecting the high backgrounds of anthropogenic radio noise as seen from space. In addition, since space-based RF lightning *location* (as opposed to mere detection) relies on multisatellite time difference of arrival (TDOA) methods (Suszcynsky et al. 2000a), it is preferable to work with narrow (a few μs) pulses.

There are essentially two classes of lightning RF pulses that are sufficiently narrow and intense to meet these two requirements. The first of these pulse types is radiated by the initiation of negative cloud-to-ground (−CG) return strokes on seawater (Jacobson and Shao 2002). The second of these pulse types is the RF emis-

Corresponding author address: Abram R. Jacobson, ISR-2, Mail Stop D436, Los Alamos National Laboratory, Los Alamos, NM 87545.
E-mail: ajacobson@lanl.gov

sion associated with an intracloud discharge process called a compact intracloud ischarge (CID; Smith et al. 1999). The CID is seen in the VHF but may sometimes precipitate a lower-frequency radiation called a narrow bipolar event (NBE; Jacobson 2003a,b; Jacobson and Light 2003; Le Vine 1980; Light and Jacobson 2002; Smith et al. 1999; Willett et al. 1989).

The CID emissions are the most intense thunderstorm emissions in the VHF and have been routinely detected from the ground (Thomas et al. 2001), from low-earth orbit (Jacobson and Light 2003; Light and Jacobson 2002; Massey and Holden 1995; Massey et al. 1998a), and from the Global Positioning System satellite constellation (Suszcynsky et al. 2000a) at 12-h orbit. Henceforth we shall use the single term NBE to refer to both the more numerous CIDs (seen in VHF) and the less numerous NBEs that are seen in lower frequencies and are precipitated by a CID. The intense RF pulse sometimes followed by an NBE is accompanied by less optical power than are the various non-NBE lightning processes (Jacobson 2003a,b; Jacobson and Light 2003; Light and Jacobson 2002). The relationship of optical output to the NBE low-frequency discharge will be explored in a separate publication; for the present, suffice it to say that the low-frequency NBEs, like their VHF instigators, tend to be dark compared to ordinary lightning. Since light output is implied by the name "lightning," evidently the NBE is an extraordinary form of lightning. Thus we shall distinguish NBEs and non-NBEs by calling all non-NBE's "ordinary lightning." Observations (Jacobson 2003a,b) are consistent with a possible role of energetic cosmic rays in the instigation of NBEs and their associated RF emissions, as proposed earlier (Gurevich et al. 1999).

Figure 1 shows (a) positive-polarity NBE, (b) negative-polarity NBE, and (c) ordinary-lightning vertical-electric-field signals as recorded by the Los Alamos Sferic-waveform Array (LASA; see section 2 below). The initial pulse is bipolar and has a duration on the order of 10 μs, much shorter than the pulses seen with typical ordinary lightning. The delayed echoes on the NBE traces (Figs. 1a and 1b) are due to ionospheric reflections and are the basis for LASA's emission-height estimates (Smith et al. 2004).

Because of its higher intensity in the VHF band, RF signals associated with NBEs will be essential to space-based RF monitoring of thunderstorms. Therefore, it is necessary to assess the NBE's utility as a remote sensing proxy for deep convection. Others have demonstrated that ordinary lightning can be a useful proxy for deep convection, albeit with systematic differences between diverse cloud regimes, for example, oceanic versus continental, pristine versus aerosol-dominated, or monsoon versus break conditions (Boccippio 2002; Boccippio et al. 1999; Nesbitt et al. 2000; Petersen and Rutledge 1998; Toracinta and Zipser 2001; Toracinta et al. 2002; Ushio et al. 2001; Williams et al. 2002; Zipser 1994; Zipser and Lutz 1994). Thus, the key question to be addressed here is the following: Do NBEs behave like ordinary lightning, and in particular, do NBEs share ordinary lightning's marked selectivity for severe tropospheric convection? If so, then NBEs might be a useful remote sensing proxy for severe convection. Or are NBEs merely an aesthetically pleasing curiosity of nature (on a par with, e.g., a "sun dog"), having little selectivity for severe convection? If the latter, then NBEs would not be a promising remote sensing observable for global monitoring of severe convection.

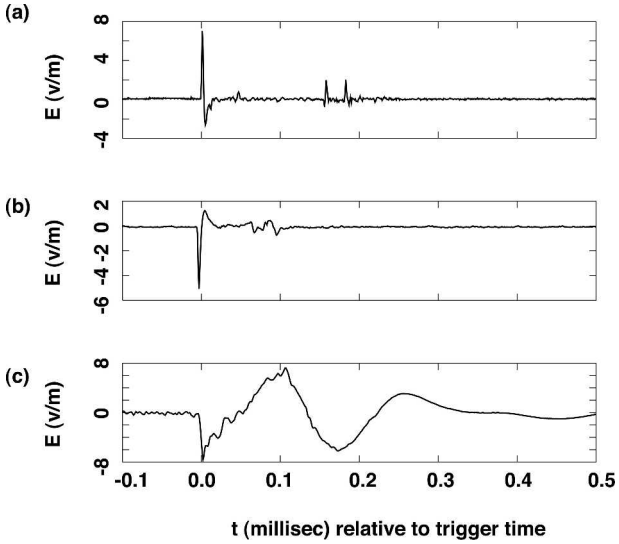

FIG. 1. Vertical-electric-field waveforms recorded by the LASA ground-based facility (see text). (a) Positive NBE followed by ionospheric reflections. (b) Negative NBE followed by ionospheric reflections. (c) Non-NBE ("ordinary") lightning signal.

2. Description of the data sources

The data used in this study comprise (i) recordings of lightning-discharge vertical-electric-field-change signals at ground level and (ii) inference of cloud-top temperature from satellite infrared cloud imagery. The data are focused on the Florida region. Specifically, the cloud imagery is stored for an 8° × 8° (longitude–latitude) box, and the lightning data are stored for a 400-km-radius circle located within that box, with both the box and the circle centered on 28°N latitude, –81.5°E longitude. Figure 2 shows the Florida area with the 400-km-radius circle superposed.

The data on lightning discharges are from LASA (Smith et al. 2002) in the Florida area during the 4-yr period 1999–2002. The array at various times during 1999–2002 (cumulatively, but not always simultaneously) comprised stations at the locations shown in Table 1. The data on any particular lightning discharge used here are accepted only if there are at least four stations participating in that particular lightning location. This allows at least four data points (waveform

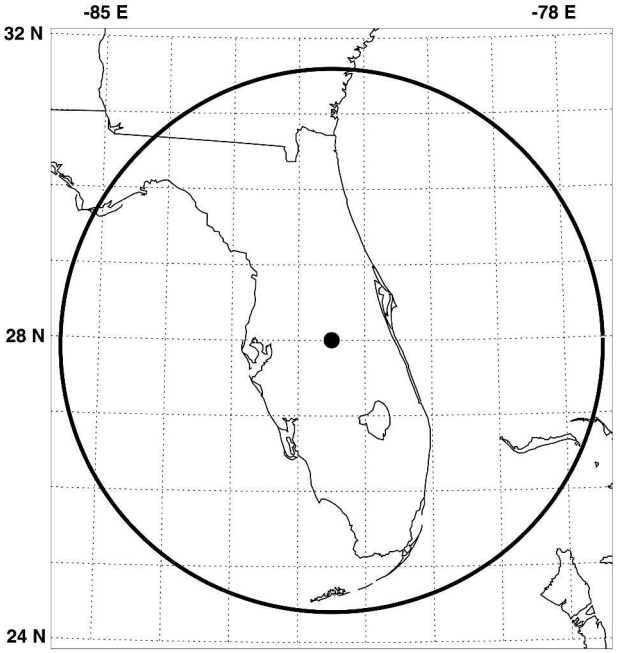

FIG. 2. Map of Florida study area, with 400-km-radius circle centered on 28.0°N, –81.5°E. The lightning-location grid extends over 8° × 8° centered on this point, with 0.2° × 0.2° pixels.

arrival times at stations) for the retrieval of three unknowns (longitude, latitude, and time of the lightning discharge). The degrees of freedom (≥1) allow assessment of the lightning-location errors and rejection of spurious solutions.

LASA is a research tool developed by the Los Alamos National Laboratory (LANL) for ground support of the Fast Onboard Recording of Transient Events (FORTE) satellite (Jacobson et al. 1999) and of the radio sensors on the GPS satellites (Suszcynsky et al. 2000a). The electric-field waveform is sampled at a rate of 1 megasample s^{-1} (so that the Nyquist bandpass is 0.5 MHz). Typically 8192 samples (8.192 millisec) of data are contained in a record for a single trigger. The LASA system returns full waveform records to the network headquarters (in Los Alamos, New Mexico) daily for analysis and attempted identification of the causative lightning process. The choices of lightning process include +NBE, −NBE, +CG, −CG, and "undetermined." The robotic identification of LASA-recorded waveforms is conservative, and most of the "undetermined" that are checked by eye appear to be probable ground strokes. For either polarity of NBE, the discharge height can often be determined (Smith et al. 2004). Both of these features—return of the full waveform and retrieval of the emission height for some NBE discharges—are unique to LASA and are not currently available in operational lightning-location systems based on signals in the low-frequency (30–300 kHz) and very low frequency (3–30 kHz) range. This ability to archive and to examine full waveforms is the reason for the LASA research facility. Table 2 indicates the number of each identified type of lightning discharges located by LASA within the 400-km-radius circle (see Fig. 2) during the 4 yr of this study. Summing over the various types of identifications, there were 3 073 907 acceptable lightning locations during the 1999–2002 period.

TABLE 1. LASA stations in Florida (cumulative over 1999–2002).

Station name (abbreviation)	Latitude (°N)	Longitude (°E)
Boca Raton (br)	26.3733	−80.1015
Cape Kennedy (kc)	28.5386	−80.6424
Tampa (ta)	28.0598	−82.4145
Fort Myers (fm)	26.6346	−82.0151
Gainesville (gv)	29.6424	−82.3472
Near Fort Myers (fy)	26.6441	−81.8687
Orlando (or)	28.5860	−81.1960
Daytona (da)	29.1891	−81.0472
Tallahassee (te)	30.4461	−84.2994
Key West (kw)	24.5816	−81.6899

The data on cloud-top temperature are derived from the Geostationary Operational Environmental Satellite-East (GOES-East) infrared (10.7-μm IR; channel 4) data made available by the National Oceanic and Atmospheric Administration (NOAA). We download the entire hemispheric image (updated typically every 15 min) and archive the image at our LASA headquarters. The data are downloaded from the National Aeronautics and Space Administration (NASA) Goddard Space Flight Center FTP Web site (ftp://rsd.gsfc.nasa.gov/) automatically at the end of each day. During the period 1999–2002, we usually, but not always, succeeded in automatically archiving the cloud imagery. The satellite data were not always available even if the download was attempted. For this and other reasons, there are substantial gaps in the IR imagery archive used in this study. Furthermore, a threshold was set to exclude entire days having <10 LASA events within the 400-km-radius circle, even if the GOES-East data were in our archive. The IR data were considered usable for a given lightning discharge only if the IR was recorded within ±15 min (900 s) of the lightning event's occurrence. Subject to these restrictions, the total number of accepted, IR-supported LASA events within the 400-km-radius circle was 1 054 836 during the period 1999–2002. This is about a third of the total number of lightning locations characterized by LASA within the 400-km-radius circle during that period. Table 3 indicates the breakout of these 1 054 836 IR-supported

TABLE 2. Number of LASA locations of various lightning types for 1999–2002. Required: four or more Florida stations participating in location.

+CG	−CG	Undetermined	+NBE	−NBE
23 991	1 697 338	1 249 338	79 068	24 172

TABLE 3. Number of LASA locations of lightning types for 1999–2002 with simultaneous GOES-East channel-4 infrared imagery. Required: four or more Florida stations participating in location.

Non-NBE (= +CG, −CG, and undetermined)	NBE (= +NBE and −NBE)	NBE (= +NBE and −NBE) with height retrieval
1 001 347	32 556	20 933

events in the overall categories of NBEs and non-NBEs, as well as the number of NBEs that provided automated emission-height retrieval (Smith et al. 2004).

3. Relation of narrow bipolar events to cloud-to-ground lightning discharges

A previous study (Suszcynsky and Heavner 2003) demonstrated two trends: First, the NBE occurrence rate statistically trends upward for Florida thunderstorms with higher flash rates of −CG or +CG lightning events. Second, the storms with higher flash rates of –CG or +CG lightning events also tend to have higher altitudes of NBE discharges. Each trend was shown to be statistically significant though with wide scatter. In the present study we further examine the spatial and temporal relationship between the CG and NBE lightning events.

To compare the behavior of NBEs and CGs, we have divided the 8° × 8° study zone (see Fig. 2) into 40 × 40 pixels (1600 pixels total), each pixel measuring 0.2° × 0.2°, or ~20 km (east–west) × 22 km (north–south). This is within a factor of 2 of the typical convective-cell size (~10 km) in either airmass thunderstorms or multicellular fronts. We have divided time into windows of duration 10 min (600 s), advanced by half a window width (5 min, or 300 s). Thus each three-dimensional spatiotemporal data pixel is spaced by 20 km (east–west) × 22 km (north–south) × 300 s. This compares with a spacing of 50 km × 50 km × 900 s used previously (Suszcynsky and Heavner 2003). The present study thus increases the three-dimensional spatiotemporal pixel-spacing density by a factor of ~30. This ought to improve the analysis' selectivity for specific life cycle periods during the development and decay of individual convective cells.

In practice, the proportion of +CGs is extremely low in Florida storms (see Table 2) compared to certain other geographical regions. This study's LASA dataset has a +CG/−CG ratio of 0.014. This is not inconsistent with a recent comprehensive study (Carey et al. 2003) of the relationship of severe storm reports to the CG polarity, which indicates that the association of predominantly positive-polarity storms to severe weather is evident in the Great Plains and upper Midwest, while Florida does not display this association. Therefore we caution that our present study, centered on Florida, cannot address the relationship of NBEs to +CGs, because the latter are not sufficiently represented in our Florida dataset.

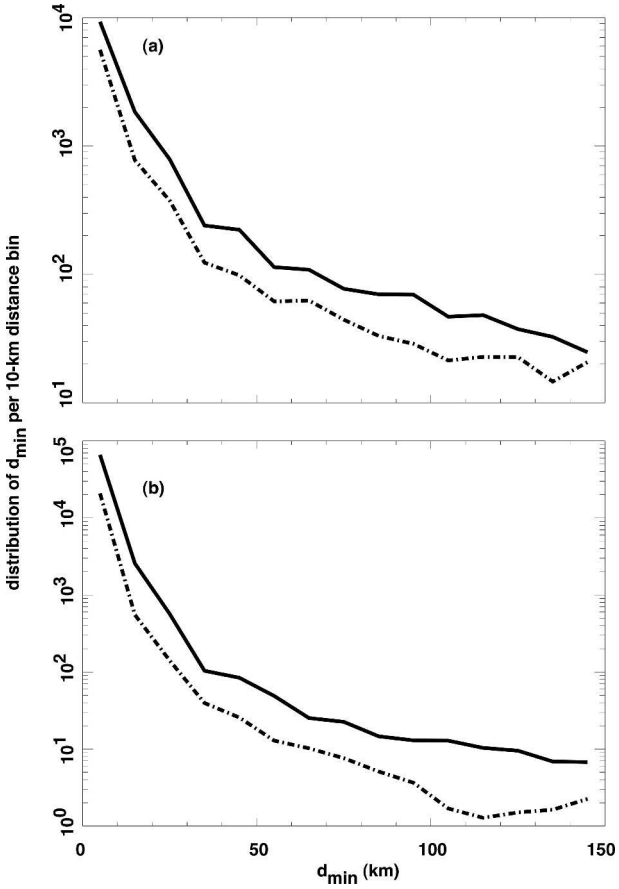

FIG. 3. Distribution of minimum distance from key lightning events to neighboring lightning events vs isotropic distance. (a) Solid curve: key events = +NBEs, neighboring events = −NBEs. Dashed curve: key events = −NBEs, neighboring events = +NBEs. (b) Solid curve: key events = +NBEs, neighboring events = non-NBEs. Dashed curve: key events = −NBEs, neighboring events = non-NBEs. The distributions have been corrected for the uneven sampling of isotropic distance (see text).

To demonstrate the spatial relationship between NBE and CG events, we first examine the minimum distance of an event of one kind to an event of another. To do this, we use a sliding 11 pixel × 11 pixel window centered on the pixel containing any particular lightning event. We tally the minimum distance from the sliding window's central pixel to the closest pixel that contains a neighbor event of a given lightning type. This results in uneven sampling of isotropic distance, so we correct for that by normalizing with the number of possible samples in each isotropic-distance bin. Figure 3 shows the bias-corrected distribution of minimum distance to simultaneous neighbors, using 10-km isotropic-distance bins. Figure 3a shows the minimum distance of one polarity of NBE to the other polarity. The solid curve is the distribution of minimum distance from +NBEs (centered in the moving 11 pixel × 11 pixel

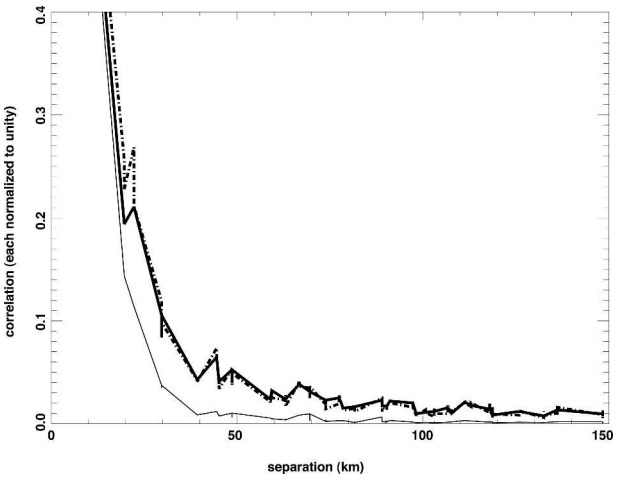

FIG. 4. Equal-time, spatial correlation functions vs isotropic separation. All curves are truncated at 0.4 even though their highest point (at zero separation) is unity. Heavy solid curve: autocorrelation function of –CG pixel occupancy. Light solid curve: autocorrelation function of +NBE pixel occupancy. Heavy dashed curve: cross-correlation function of –CG with +NBE pixel occupancies, multiplied by factor 1/0.29 to compensate for 29% correlation at zero separation. The finescale irregularities are caused by anisotropies (see text).

window) to neighboring –NBEs. The dashed curve is the distribution of minimum distance from −NBEs (centered in the moving 11 pixel × 11 pixel window) to neighboring +NBEs. It apparently is rare to have any spatial association between simultaneous NBEs of opposite polarity. That is, each storm containing NBEs tends to contain only NBEs consistently of one polarity or another, but not both. The total number of +NBEs in this study is 79 068 (see Table 2), but the percentage of these +NBEs associated with simultaneous –NBEs within 150-km distance is only less than 15% (see Fig. 3a, solid curve). A similar conclusion holds for –NBEs (see Fig. 3a, dashed curve). Despite the tendency of NBE-producing storms to produce only one polarity of NBEs, the few cases (<15%) of storms that produce both polarities tend to place them in close proximity (same pixel; see Fig. 3a).

Figure 3b shows the minimum distance from +NBEs (solid curve) and from –NBEs (dashed curve) to non-NBEs (+CG, −CG, and undetermined events). Each polarity of NBE is overwhelmingly likely to occur in a pixel that simultaneously contains at least one non-NBE lightning event. Thus, almost whenever NBEs occur, they do so in pixels containing "ordinary lightning." Thus NBEs are not an isolated phenomenon set apart from ordinary lightning, but occur almost without exception in places where ordinary lightning simultaneously (within 10 min) occurs.

The next step in testing the spatial relationship between NBEs and ordinary lightning is to estimate the covariances versus spatial and temporal separation. We use the same 11 pixel × 11 pixel sliding window centered on the pixel containing the key event. We look for neighbors of the key event in all 121 pixels in the 11 pixel × 11 pixel sliding window. However, rather than note the minimum distance to a neighbor, we take the product of the central-pixel population of key events times the populations of all 121 pixels in the sliding window. This gives 121 products, representing discrete sampling of different separations. We then sum that product matrix over all 300-s time steps and over all days in the 4-yr period 1999–2002. Finally, we reorder the 121-element matrix elements by isotropic distance from the key event.

Based on the summed population-product matrix, we calculate the normalized correlation versus isotropic separation. Because Florida (see Fig. 2) is not isotropic but rather is a peninsula, and tends to impose some degree of north–south elongation on the storm activity, the spatial correlation shows slight departures from isotropy.

Figure 4 shows three correlation functions, truncated to highlight the correlation range 0.0 to 0.4. The heavy solid curve is the autocorrelation of –CG populations, normalized to unity at zero separation. The light curve is the autocorrelation of +NBE populations, also normalized to unity at zero separation. The heavy dashed curve is the cross correlation of –CG populations with +NBE populations. The cross correlation's zero-separation value is only 0.29 (see Table 4), but the heavy dashed curve has been artificially amplified by 1/0.29 to allow ready comparison with the two autocorrelation functions.

The finescale irregularities in all three curves in Fig. 4 are due to the slight anisotropies in the correlation matrix. Despite this anisotropy, all three correlations fall off clearly with increasing isotropic separation. The –CG autocorrelation (heavy solid curve) is wider than the +NBE autocorrelation (light curve), below the 0.2 correlation level. The cross correlation mimics the wider autocorrelation. These relationships indicate that NBEs tend to occur in spatially tighter subzones of the storms compared to ordinary lightning. The 0.29 cross correlation of +NBEs with –CGs in Florida is highly significant, as the statistical noise (tail value at right end of heavy dashed curve) is only <0.02. The

TABLE 4. Equal-time, zero-separation, pixel-population correlation coefficients. Data used are the full 1999–2002 dataset with four or more Florida stations participating in location (see Table 2).

Undetermined +NBE	Undetermined −NBE	Undetermined −CG	+NBE, −NBE	−CG, +NBE	−CG, −NBE
0.25	0.26	0.47	0.11	0.29	0.16

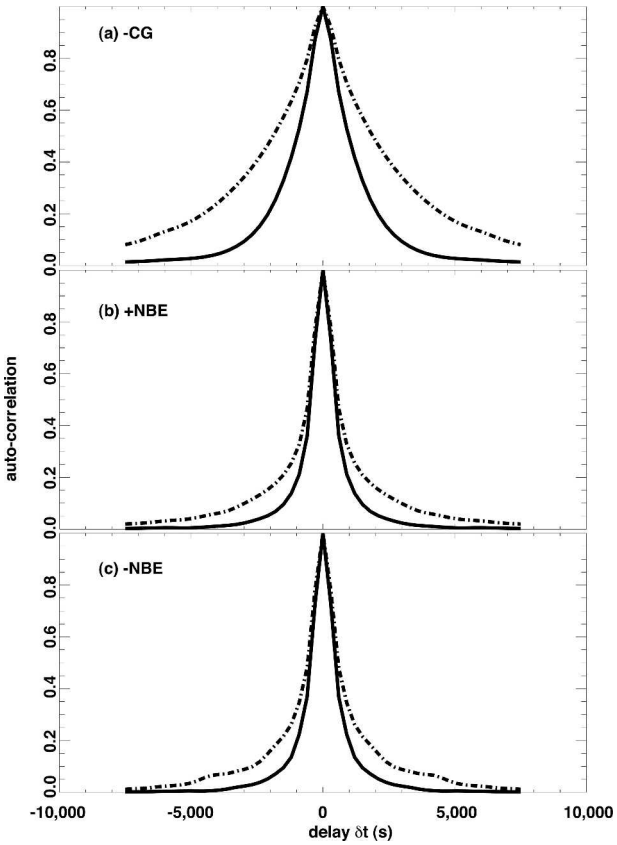

FIG. 5. Zero-separation, temporal autocorrelation functions for (a) –CG pixel occupancies, (b) +NBE pixel occupancies, and (c) –NBE pixel occupancies. Solid curves: without further spatial averaging. Dashed curves: with prior spatial smoothing by 5 pixels × 5 pixels (~100 km × 100 km).

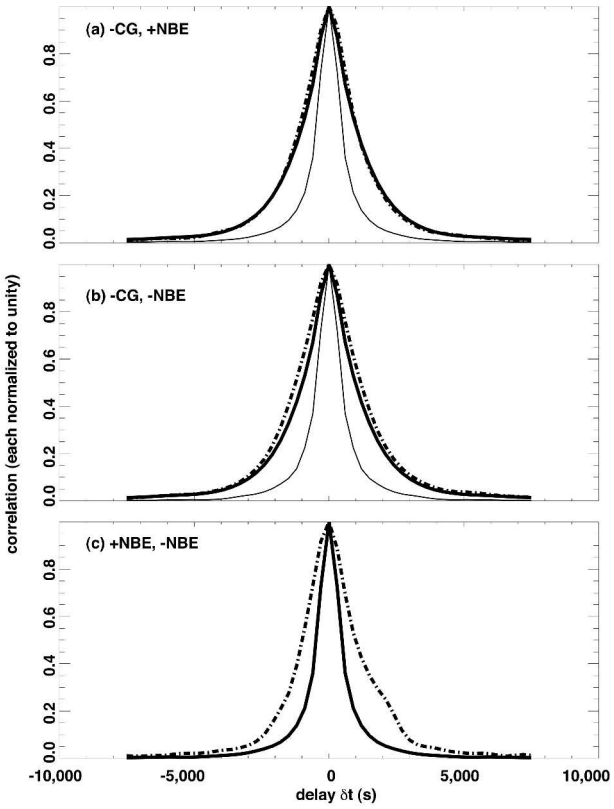

FIG. 6. Two autocorrelation functions repeated from Fig. 5 (heavy and light solid curves) and one cross-correlation function (heavy dashed curve), for (a) –CGs and lagged +NBEs (multiplied by factor 1/0.29), (b) –CGs with lagged –NBEs (multiplied by factor of 1/0.16), and (c) +NBEs with lagged –NBEs (multiplied by factor of 1/0.11). The light solid curve in (c) is almost identical to, and therefore covered by, the heavy solid curve.

significant, but partial, cross correlation is consistent with earlier findings of a statistical, though not case-by-case, proportionality between CG flash rates and NBE event rates (Suszcynsky and Heavner 2003). The behavior of the −NBE pixel populations (not shown) is similar to that of the +NBEs, although the −NBEs' peak correlation with –CGs is only 0.16 (see Table 4). The –NBE autocorrelation is almost identical in shape and width with the +NBE autocorrelation (Fig. 3, light solid curve). All the zero-separation correlation coefficients are listed in Table 4.

The results in Figs. 3 and 4 have shown the equal-time correlations as a function of spatial separation. Now we reverse the procedure and examine the zero-separation correlations as a function of temporal separation. Figure 5 shows the temporal autocorrelations for (a) –CGs, (b) +NBEs, and (c) –NBEs. In each panel, the solid curve is without any spatial smoothing, while the dashed curve is with 5 pixel × 5 pixel (approximately 100 km) spatial smoothing. The half-width to $1/e$ for –CGs is about 2500 s without spatial 100-km smoothing, and about twice that with spatial 100-km smoothing. The half-width to $1/e$ for each type of NBE is about 1200 s without spatial 100-km smoothing, and only about 25% more with spatial 100-km smoothing. Two features are apparent: First, the duration of NBE occurrences during a given storm tends to be only half the duration of –CG occurrences in the same storm. Second, the distribution of –CGs is twofold wider in time if we first average over 100 km spatially, whereas the distribution of NBEs undergoes 25% further widening in time. This indicates that –CGs appear in more phases of a developing/advecting storm complex than do NBEs (of either polarity.)

Lagged (as a function of lag δt) correlations can also address whether one type of lightning event tends to precede, or follow, another type during the development of storms. Figure 6 shows (heavy dashed curve) the cross-correlation of (a) $-\mathrm{CG}(t)$ with $+\mathrm{NBE}(t+\delta t)$, (b) $-\mathrm{CG}(t)$ with $-\mathrm{NBE}(t+\delta t)$, and (c) $+\mathrm{NBE}(t)$ with $-\mathrm{NBE}(t+\delta t)$. In each panel the heavy solid curve is the first type's autocorrelation, the light curve is the second type's autocorrelation, and the heavy dashed curve is the cross correlation. The latter is artificially multiplied by the inverse of the cross-correlation coef-

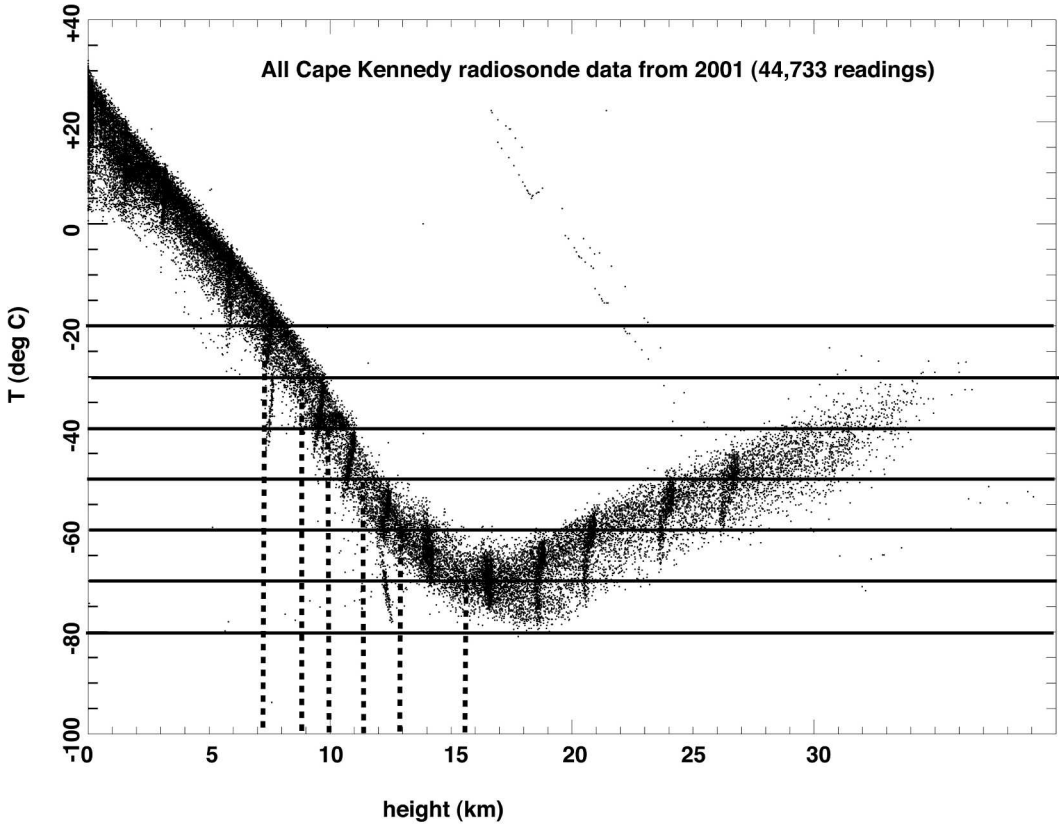

FIG. 7. Cape Kennedy radiosonde temperature measurements vs height for all soundings during 2001. Spurious artifacts are included. Data from NOAA/Forecast Systems Laboratory (see text).

ficient (see Table 4) to allow ready comparison to the autocorrelation functions. The autocorrelations in Fig. 6 are the same as the autocorrelations in Fig. 5 and are repeated to provide a comparison to the cross correlations.

Figure 6 indicates that there is no systematic lag of NBEs (of either polarity) with respect to –CGs. Although NBEs (of either polarity) occur during a smaller duration of the storm life cycle than do –CGs, the NBE occurrences are not systematically advanced or retarded with respect to the temporal centroid of –CGs. Similarly, to the small extent that –NBEs coexist with +NBEs (correlation: 11%), they have no systematic lag relationship (Fig. 6c).

4. Comparison of lightning incidence to cloud-top temperature data

The purpose of this section is to determine whether NBEs behave as do –CGs with respect to their spatial relationship to clouds. Ordinary lightning is far more likely to be accompanied by high (i.e., cold) cloud tops (Williams 2001) than to be accompanied by low (i.e., relatively warm) cloud tops. Do NBEs behave similarly? We answer this with infrared cloud maps. These cloud maps at 10.7 μm (GOES-East, IR channel 4) reveal the cloud-top temperature. The cloud-top temperature then serves as a crude cloud-top altimeter, assuming that the inferred temperature is in equilibrium with the environmental thermocline. This altimetry can be performed only in the monotonic portion of the thermocline, from ground to the tropopause. It is not expected that thunderclouds will occur in equilibrium above the tropopause, although a few kilometers of overshoot can occur transiently for exceptionally vigorous convection (Williams 2001). At any rate, for cloud parcels that are in vertical motion and hence not in equilibrium with their surroundings, the altitude estimate from cloud-top temperature is erroneous.

The thermocline varies both diurnally and seasonally. Figure 7 shows temperature versus height from all radiosondes launched out of Cape Kennedy, Florida, during 2001, regardless of local time and season. The radiosonde observations are provided by the NOAA/Forecast Systems Laboratory (http://raob.fsl.noaa.gov). Each of the 44 733 dots in Fig. 7 is a reported temperature. The dots follow a well-defined and reproducible thermocline. Some anomalous outliers are obvious; all 2001 data are included without editing, including points with obvious errors. Superimposed on the data are iso-

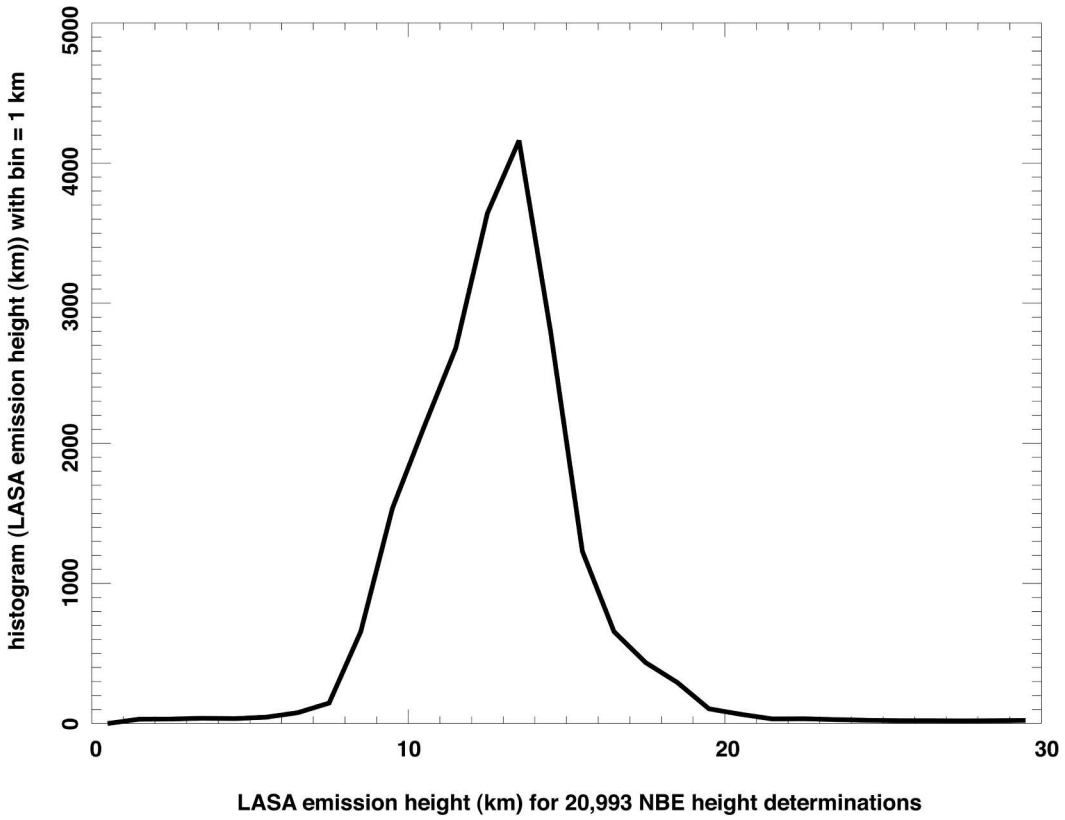

FIG. 8. Distribution of NBE emission height for 20 993 NBE waveforms that allowed automated retrieval of ionospheric and emission heights (see text).

therms (horizontal lines) from –20° to –80°C, in steps of 10°C. Each isotherm's intersection with the observed thermocline is marked by a dashed vertical line at constant altitude. It is seen that the temperature tropopause occurs around ~15 km altitude and at a temperature around –70°C. Thus it would not be expected to see thunderclouds above 15 km in equilibrium with their environment.

The first question is, Do the NBEs occur at heights that are consistent with their being in the troposphere? If not, it would be difficult to associate them with thunderstorm phenomena. The NBE waveform often permits the automated retrieval of emission height (Smith et al. 2004). This was possible in about ⅔ of the NBEs used in this analysis with IR-imagery support (see Table 3). Figure 8 shows the distribution of inferred NBE emission height based on automated processing of the waveform. The distribution peaks at 13–14-km altitude. Over 80% of the NBEs are emitted below 15 km. However, the <20% of NBEs in this distribution that are emitted in the range 15–20-km altitude are unlikely to be completely explainable as measurement artifacts. We believe our altitude-measurement uncertainties are <2 km, so it is likely that at least some of these events are truly occurring above the nominal tropopause. It remains unclear whether these high-altitude NBEs occur in clear air above the cloud tops [as in "blue jets" (Wescott et al. 1995)] or occur in overshooting clouds that transiently exceed the equilibrium tropopause height (Williams 2001).

Having determined that the NBEs tend to occur in the upper troposphere, we now examine what their relationship is with cloud heights as inferred from the cloud-top temperature. For this purpose, we do not use the lightning-event pixelation but instead use the exact observed location of each lightning event. We use the pixels of the GOES-East image (which do *not* coincide with our $0.2° \times 0.2°$ lightning pixelation) and compute the inferred cloud-top temperature for those pixels. For each lightning event detected by LASA, we gather all the image pixels whose centers lie within both 30- and 100-km-radius circles centered on the lightning location. We then build two statistics from the cloud-top temperatures within each of these circles: First, we tally the full distribution of cloud-top temperatures within the circle. Second, we tally the coldest cloud-top temperature within the circle. These two statistics are then accumulated over the entirety of LASA-located lightning events (see Table 3) for which there is GOES-East imagery.

Figure 9 shows histograms of the distribution of cloud-top temperatures proximal to lightning, summed

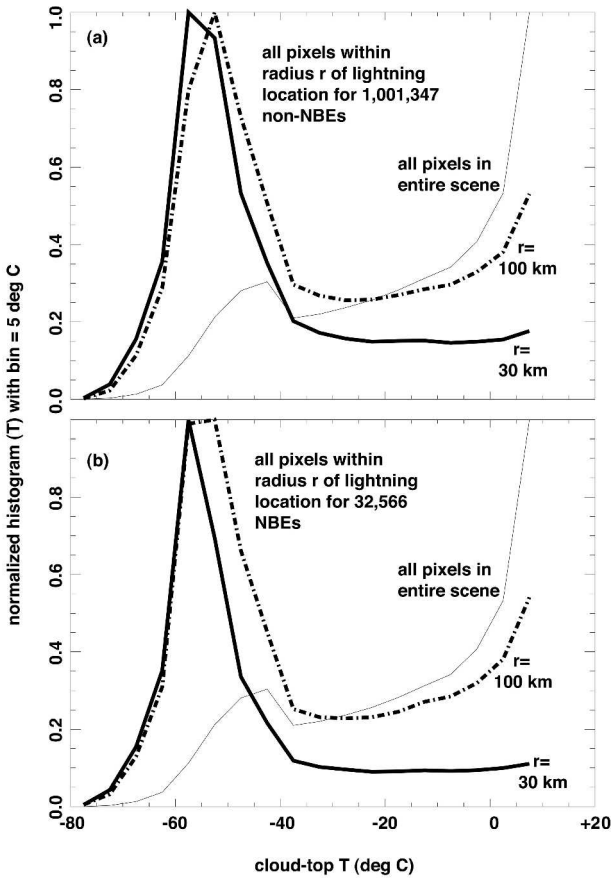

FIG. 9. Distribution of cloud-top temperatures inferred from GOES-East IR (10.7 μm) imagery during times in 1999–2002 in which there was LASA data. Light curve: background cloud distribution over entire Florida-area subimage (see Fig. 2). Heavy solid curve: cloud distribution within 30-km proximity to each lightning event. Heavy dashed curve: cloud distribution within 100-km proximity to each lightning event. (a) For non-NBE lightning and (b) for NBE lightning (both polarities).

over all the IR images in the archive. The light curve is for the background distribution over all pixels in the entire scene, regardless of proximity to lightning locations. The heavy solid curve is for those pixels within a 30-km-radius circle proximal to each lightning event. The heavy dashed curve is for those pixels within a 100-km-radius circle proximal to each lightning event. The lightning events in Fig. 9a are non-NBEs (+CG, −CG, and undetermined), while those in Fig. 9b are the NBEs (of both polarities summed together).

First consider the background temperature distribution (light line) in both panels of Fig. 9. Obviously it is the same curve in both Figs. 9a and 9b, because it is not conditioned by proximity to lightning. The steeply rising feature at the far right (high temperature) is the transition to clear skies. The smaller hump at –40° to –50°C is the cloud signature. This cloud signature has a tail going out to –70°C, roughly as we would expect (see the radiosonde data in Fig. 7) for deep convection.

Next, consider the distribution of cloud-top temperatures in proximity to either non-NBEs (Fig. 9a) or NBEs (Fig. 9b). The peak for either 30- or 100-km proximity is located on the cold (left) tail of the background distribution, near –50° to –60°C. According to the radiosonde thermocline (Fig. 7), that corresponds to altitudes around 12 km. That is within the peak of the NBE altitude distribution inferred from the waveform data (Fig. 8), so the two independent ways of constraining cloud height seem not to be radically inconsistent. For both non-NBEs (Fig. 9a) and NBEs (Fig. 9b), the distributions for $r = 30$ km are colder than those for $r = 100$ km. This is reasonable, in that the farther away from the lightning location one allows the cloud pixel to be accumulated in the statistic, the more chance of including shallower (lower) clouds that are near, but not immediately associated with, the lightning. This also explains the higher "bridge" value for $r = 100$ km in the transition region (−40° to 0°C). Farther from the lightning, there is more low cloud, broken cloud, or even clear sky.

Given that lightning can occur in compact updraft cells whose transverse size (<10 km) is not well resolved in GOES imagery, the use of 30-km-radius—and even more so 100-km-radius—circles around a given lightning event inevitably tends to include portions of the image that are not directly pertinent to the electrification/lightning process. In Fig. 10, we show the distributions of the *single coldest* cloud pixel within these two radii. These single-coldest-pixel distributions are much narrower than the distributions of Fig. 9 and entirely lack the "bridge" feature at $T > -40$°C. The centroid of the peak for either non-NBEs (Fig. 10a) or NBEs (Fig. 10b) is around –60°C. This corresponds to the 13-km height on the radiosonde data (Fig. 7). Notice also that the single-coldest-pixel distribution remains significant right out to –70°C, corresponding to the nominal tropopause.

The cloud-top-temperature distributions in both Figs. 9 and 10 indicate that, as regards affinity for cold cloud tops, NBEs behave roughly as do ordinary lightning events. Both non-NBEs and NBEs are highly selective for being near the coldest cloud tops possible, up to the limit imposed by the tropopause temperature. Both non-NBEs and NBEs are highly unlikely to occur within cloud environments warmer than –40°C. This is consistent with the consensus of observations reviewed elsewhere (Williams 2001).

5. Summary and conclusions

We have examined the relationship of NBE lightning to ordinary (non-NBE) lightning, using the same detection system (LASA) for an unbiased comparison, over 4 yr of observations within a tight geographical study area centered on Florida. This dataset comprises about three million lightning events. We have compared the LASA data with cloud-top-temperature inferences

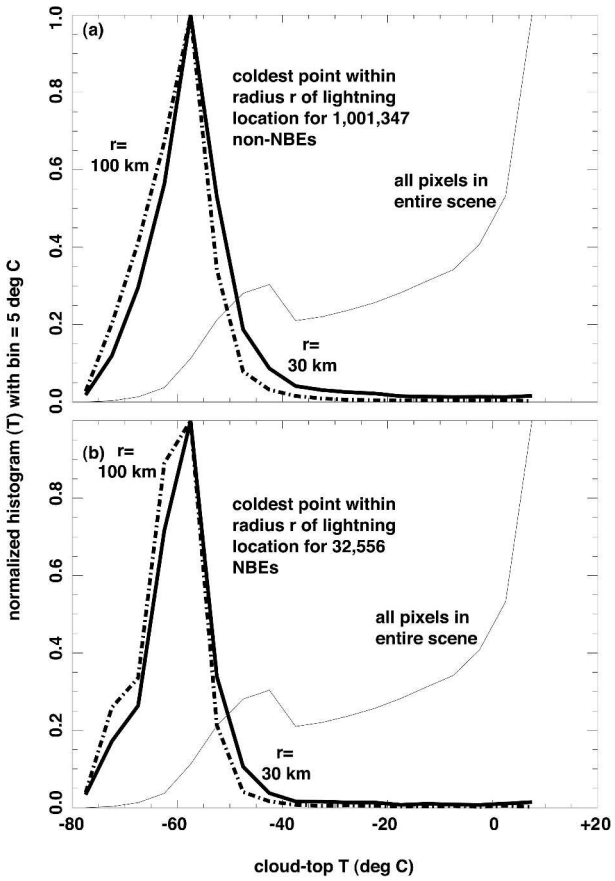

FIG. 10. Light curve is identical to that in Fig. 9, but heavy curves are distributions of *minimum* cloud-top temperature proximal to lightning events, within $r = 30$ km (heavy solid curve) and within $r = 100$ km (heavy dashed curve). (a) Lightning = non-NBEs; (b) lightning = NBEs.

from GOES-East IR images that are recorded within 15 min of any given lightning event. The IR-supported lightning events number over one million. Our observations lead to the following conclusions:

1) When a given thunderstorm gives rise to NBE discharges, the polarity of the discharge tends to be consistent for that storm. That is, a given storm is usually associated purely with +NBEs or purely with –NBEs, but not both (see Fig. 3a).
2) When a given thunderstorm gives rise to NBE discharges (regardless of polarity), that storm also gives rise to ordinary (non-NBE) lightning discharges (see Fig. 3b).
3) Spatially, NBEs occupy a more compact portion of a thunderstorm than do non-NBEs (see Fig. 4); +NBEs and –NBEs are similarly compact in their appearance, though not in the same storms.
4) During the development and advection of a thunderstorm, the non-NBEs are present for about twice as long as are the NBEs (see Fig. 5). This does not depend on NBE polarity.
5) Within thunderstorms, NBEs neither consistently precede nor consistently follow the centroid of non-NBE occurrences (see Fig. 6).
6) Most NBEs occur at altitudes within the upper troposphere. Fewer than 20% occur above the nominal tropopause, and virtually none above 20 km.
7) The distribution of cloud-top temperatures proximal to the locations of both NBEs and non-NBEs is peaked at –50° to –60°C (see Fig. 9), corresponding to cloud-top heights in the upper troposphere. The cloud-top-temperature distribution for NBEs is essentially similar to the distribution for non-NBEs.
8) The distribution of single-coldest-pixel cloud-top temperatures proximal to the locations of both NBEs and non-NBEs is peaked at –60°C (see Fig. 10). The single-coldest-pixel cloud-top-temperature distribution proximal to NBEs is essentially similar to the distribution proximal to non-NBEs. Both NBEs and non-NBEs are almost never seen in cloud systems for which all cloud-top temperatures are warmer than –40°C within 30 km proximal to the lightning event.

In summary, the behavior of NBEs appears to be essentially the same as the behavior of non-NBEs, as regards selectivity for deep convective-cloud structures. As regards the timing and spatial relation of NBEs to non-NBEs in storms that contain both, NBE occurrence tends to cover less of the spatial extent or temporal lifetime of the storm. NBE occurrence does not appear to be a consistent precursor of non-NBE occurrence, and vice versa. Therefore, in view of what we have found, it seems reasonable to assume that the extensive literature on the meteorological setting of "ordinary" lightning might also apply to NBE lightning. In particular, it appears reasonable to assume that NBEs as a remote sensing proxy of severe convection might have a utility comparable to that of ordinary lightning, albeit in the context of radio VHF, not optical, detection techniques.

A limitation of this study is that Florida has too few +CGs to allow a determination of the relationship of NBEs and +CGs. Future work in locations other than Florida, for example, in the Great Plains, will be required to address this question.

Acknowledgments. This work was conducted under the auspices of the U.S. Department of Energy, with support from the LANL/LDRD program. The LASA facility is the product of many years of effort by many staff, postdocs, and students at Los Alamos, without whose contributions the present work would not have been possible.

REFERENCES

Boccippio, D. J., 2002: Lightning scaling relations revisited. *J. Atmos. Sci.,* **59,** 1086–1104.

——, W. J. Koshak, H. J. Christian, and S. J. Goodman, 1999: Land–ocean differences in LIS and OTD tropical lightning

observations. *Proc. 11th Int. Conf. on Atmospheric Electricity*, Huntsville, AL, National Aeronautics and Space Administration, 734–737.

——, K. Driscoll, W. Koshak, R. Blakeslee, W. Boeck, D. Buechler, H. Christian, and S. Goodman, 2000: The Optical Transient Detector (OTD): Instrument characteristics and cross-sensor validation. *J. Atmos. Oceanic Technol.,* **17,** 441–458.

Carey, L. D., S. A. Rutledge, and W. A. Petersen, 2003: The relationship between severe storm reports and cloud-to-ground lightning polarity in the contiguous United States from 1989 to 1998. *Mon. Wea. Rev.,* **131,** 1211–1228.

Christian, H. J., and Coauthors, 1999a: Global frequency and distribution of lightning as observed by the Optical Transient Detector (OTD). *Proc. 11th Int. Conf. on Atmospheric Electricity*, Huntsville, AL, National Aeronautics and Space Administration, 726–729.

——, and Coauthors, 1999b: The Lightning Imaging Sensor. *Proc. 11th Int. Conf. on Atmospheric Electricity*, Huntsville, AL, Global Hydrology and Climate Center, NASA Marshall Space Flight Center.

Gurevich, A. V., K. P. Zybin, and R. A. Roussel-Dupré, 1999: Lightning initiation by simultaneous effect of runaway breakdown and cosmic ray showers. *Phys. Lett.,* **A254,** 79–87.

Jacobson, A. R., 2003a: Relationship of intracloud-lightning radiofrequency power to lightning-storm height, as observed by the FORTE satellite. *J. Geophys. Res.,* **108,** 4204, doi:1029/2002JD002956.

——, 2003b: How do the strongest radio pulses from thunderstorms relate to lightning flashes? *J. Geophys. Res.,* **108,** 4778, doi:10.1029/2003JD003936.

——, and X.-M. Shao, 2002: FORTE satellite observations of very narrow radiofrequency pulses associated with the initiation of negative cloud-to-ground lightning strokes. *J. Geophys. Res.,* **107,** 4661, doi:10.1029/2001JD001542.

——, and T. E. L. Light, 2003: Bimodal radiofrequency pulse distribution of intracloud-lightning signals recorded by the FORTE satellite. *J. Geophys. Res.,* **108,** 4266, doi:10.1029/2002JD002613.

——, S. O. Knox, R. Franz, and D. C. Enemark, 1999: FORTE observations of lightning radio-frequency signatures: Capabilities and basic results. *Radio Sci.,* **34,** 337–354.

——, K. L. Cummins, M. Carter, P. Klingner, D. Roussel-Dupré, and S. O. Knox, 2000: FORTE radio-frequency observations of lightning strokes detected by the National Lightning Detection Network. *J. Geophys. Res.,* **105,** 15 653–15 662.

Kirkland, M. W., D. M. Suszcynsky, J. L. L. Guillen, and J. L. Green, 2001: Optical observations of terrestrial lightning by the FORTE satellite photodiode detector. *J. Geophys. Res.,* **106,** 33 499–33 509.

Le Vine, D. M., 1980: Sources of the strongest rf radiation from lightning. *J. Geophys. Res.,* **85,** 4091–4095.

Light, T. E. L., and A. R. Jacobson, 2002: Characteristics of impulsive VHF lightning observed by the FORTE satellite. *J. Geophys. Res.,* **107,** 4756, doi:10.1029/2001JD001585.

Massey, R. S., and D. N. Holden, 1995: Phenomenology of transionospheric pulse pairs. *Radio Sci.,* **30,** 1645–1659.

——, ——, and X.-M. Shao, 1998a: Phenomenology of transionospheric pulse pairs: Further observations. *Radio Sci.,* **33,** 1755–1761.

——, S. O. Knox, R. C. Franz, D. N. Holden, and C. T. Rhodes, 1998b: Measurements of transionospheric radio propagation parameters using the FORTE satellite. *Radio Sci.,* **33,** 1739–1753.

Nesbitt, S. W., E. J. Zipser, and D. J. Cecil, 2000: A census of precipitation features in the Tropics using TRMM: Radar, ice scattering, and lightning observations. *J. Climate,* **13,** 4087–4106.

Petersen, W. A., and S. A. Rutledge, 1998: On the relationship between cloud-to-ground lightning and convective rainfall. *J. Geophys. Res.,* **103,** 14 025–14 040.

Roussel-Dupré, R. A., A. R. Jacobson, and L. A. Triplett, 2001: Analysis of FORTE data to extract ionospheric parameters. *Radio Sci.,* **36,** 1615–1630.

Shao, X.-M., and A. R. Jacobson, 2001: Polarization observations of broadband VHF signals by the FORTE satellite. *Radio Sci.,* **36,** 1573–1589.

——, and ——, 2002: Polarization observations of lightning-produced VHF emissions by the FORTE satellite. *J. Geophys. Res.,* **107,** 4430, doi:10/1029/2001JD001018.

Smith, D. A., and Coauthors, 1999: A distinct class of isolated intracloud lightning discharges and their associated radio emissions. *J. Geophys. Res.,* **104,** 4189–4212.

——, K. B. Eack, J. Harlin, M. J. Heavner, A. R. Jacobson, R. S. Massey, X. M. Shao, and K. C. Wiens, 2002: The Los Alamos Sferic Array: A research tool for lightning investigations. *J. Geophys. Res.,* **107,** 4183, doi:10.1029/2001JD000502.

——, M. J. Heavner, A. R. Jacobson, X. M. Shao, R. S. Massey, R. J. Sheldon, and K. C. Wiens, 2004: A method for determining intracloud lightning and ionospheric heights from VLF/LF electric field records. *Radio Sci.,* **39,** RS1010, doi:10.1029/2002RS002790.

Suszcynsky, D. M., and M. J. Heavner, 2003: Narrow bipolar events as indicators of thunderstorm convective strength. *Geophys. Res. Lett.,* **30,** 1879, doi:10.1029/2003GL017834.

——, A. Jacobson, J. Fitzgerald, C. Rhodes, E. Tech, and D. Roussel-Dupre, 2000a: Satellite-based global lightning and severe storm monitoring using VHF receivers. *Eos, Trans. Amer. Geophys. Union,* **81,** F91.

——, M. W. Kirkland, A. R. Jacobson, R. C. Franz, S. O. Knox, J. L. L. Guillen, and J. L. Green, 2000b: FORTE observations of simultaneous VHF and optical emissions from lightning: Basic phenomenology. *J. Geophys. Res.,* **105,** 2191–2201.

——, T. E. Light, S. Davis, M. W. Kirkland, J. L. Green, and J. Guillen, 2001: Coordinated observations of optical lightning from space using the FORTE photodiode detector and CCD imager. *J. Geophys. Res.,* **106,** 17 897–17 906.

Thomas, R. J., P. R. Krehbiel, W. Rison, T. Hamlin, J. Harlin, and D. Shown, 2001: Observations of VHF source powers radiated by lightning. *Geophys. Res. Lett.,* **28,** 143–146.

Toracinta, E. R., and E. Zipser, 2001: Lightning and SSM/I-ice-scattering mesoscale convective systems in the global Tropics. *J. Appl. Meteor.,* **40,** 983–1002.

——, D. J. Cecil, E. J. Zipser, and S. W. Nesbitt, 2002: Radar, passive microwave, and lightning characteristics of precipitating systems in the tropics. *Mon. Wea. Rev.,* **130,** 802–824.

Ushio, T., S. J. Heckman, D. J. Boccippio, H. J. Christian, and Z.-I. Kawasaki, 2001: A survey of thunderstorm flash rates compared to cloud top height using TRMM satellite data. *J. Geophys. Res.,* **106,** 24 089–24 095.

Wescott, E. M., D. D. Sentman, D. Osborn, D. L. Hampton, and M. Heavner, 1995: Preliminary results from the Sprites94 aircraft campaign: Blue Jets. *Geophys. Res. Lett.,* **22,** 1209–1212.

Willett, J. C., J. C. Bailey, and E. P. Krider, 1989: A class of unusual lightning electric field waveforms with very strong high-frequency radiation. *J. Geophys. Res.,* **94,** 16 255–16 267.

Williams, E. R., 2001: The electrification of severe storms. *Severe Convective Storms, Meteor. Monogr.,* No. 50, Amer. Meteor. Soc., 527–561.

——, and Coauthors, 2002: Contrasting convective regimes over the Amazon: Implications for cloud electrification. *J. Geophys. Res.,* **107,** 8082, doi:10.1029/2001JD000380.

Zipser, E. J., 1994: Deep cumulonimbus cloud systems in the Tropics with and without lightning. *Mon. Wea. Rev.,* **122,** 1837–1851.

——, and K. R. Lutz, 1994: The vertical profile of radar reflectivity of convective cells: A strong indicator of storm intensity and lightning probability? *Mon. Wea. Rev.,* **122,** 1751–1759.